Journal of Vacuum Science and Technology A

RESEARCH ARTICLE | JANUARY 31 2024

Plasma nitridation for atomic layer etching of Ni

Special Collection: Celebrating the Achievements and Life of Joe Greene

Taylor G. Smith ; Ali M. Ali ; Jean-François de Marneffe ; Jane P. Chang

J. Vac. Sci. Technol. A 42, 022602 (2024)
https://doi.org/10.1116/6.0003263

JVST A
Journal of Vacuum Science & Technology A

ARTICLE

pubs.aip.org/avs/jva

Plasma nitridation for atomic layer etching of Ni

Cite as: J. Vac. Sci. Technol. A 42, 022602 (2024); doi: 10.1116/6.0003263
Submitted: 30 October 2023 · Accepted: 3 January 2024 ·
Published Online: 31 January 2024

Taylor G. Smith,[1] Ali M. Ali,[2,3] Jean-François de Marneffe,[2] and Jane P. Chang[1,a)]

AFFILIATIONS

[1]Department of Chemical and Biomolecular Engineering, University of California, Los Angeles, California 90095
[2]Imec v.z.w., Kapeldreef 75, B-3001 Leuven, Belgium
[3]Department of Chemistry, K.U. Leuven, Celestijnenlaan 200E, B-3001 Leuven, Belgium

Note: This paper is part of the Special Topic Collection Celebrating the Achievements and Life of Joe Greene.
[a)]**Electronic mail:** jpchang@ucla.edu

ABSTRACT

Nickel (Ni) and its alloys are important multifunctional materials for the fabrication of integrated circuits, as either the absorber for the extreme ultraviolet lithography masks and/or interconnect metals at the nanometer scale. However, these applications require that Ni to be patterned controllably, selectively, and anisotropically—requirements that can only be met with a plasma based atomic layer etch (ALE) process. In this work, a plasma-thermal ALE approach is developed to pattern Ni, utilizing a nitrogen plasma to form Ni_xN at the surface, formic acid (FA) vapor to selectively remove the Ni_xN layer, and a low-energy Ar^+ sputter process to remove carbon residue left by the FA prior to the subsequent nitridation step. This three step ALE process was shown effective to etch Ni with a rate of 1.3 ± 0.17 nm/cycle while maintaining surface smoothness.

I. INTRODUCTION

Nickel (Ni) has attracted significant attention in recent years for its uses in nanofabrication. Ni and its alloys have been considered absorber layers for extreme ultraviolet (EUV) photolithography masks due to their high extinction coefficients at the 13.5 nm wavelength, a property that allows for thinner absorber layers that reduce shadowing effects.[1,2] Ni_xAl_y alloys have also been investigated as replacements for Cu interconnects at the smallest linewidths.[3,4] Successfully integrating and etching Ni requires a balance of high selectivity, low sidewall redeposition, and controllable etch rates. Atomic layer etch (ALE) has emerged as a potential method of satisfying these requirements to pattern metals such as Ni,[5,6] Co,[7–9] Cu,[10–12] Fe,[8,9,13,14] Pd,[8,9,15,16] Pt,[8,9] and Ru.[17]

ALE is a cyclic process that involves alternating, self-limiting reactions to remove material controllably and selectively. In the first half-cycle of an ALE process, the surface is modified using plasma or a reactive vapor. In the second half-cycle, the modified layer is removed through sputtering, ligand exchange, or heating.[18,19] Importantly, the second half reaction must remove only the modified surface layer selective to the unmodified underlying material. This is achieved by leveraging differences in the sputter threshold energy, Gibbs free energy of reaction, or vapor pressure that exist between the modified surface and the underlying material. In this work, a hybrid plasma-thermal ALE process—illustrated in Fig. 1—is adopted. This plasma-thermal approach uses plasma to modify the metal surface [Fig. 1(b)] and an organic vapor, such as formic acid (FA) to remove the modified layer [Fig. 1(c)]. The plasma step imparts directionality by ion bombardment, allowing for anisotropic profiles. The thermal step is more selective to the modified layer than Ar sputtering, which can damage hardmasks and unintentionally remove the underlying metal.

Previous work showing ALE of Ni relied on the oxygen plasma modification of the surface followed by the removal of the oxide layer using FA vapor.[5,20] However, the oxygen plasma chemistry presents some issues for EUV absorber layer applications. The absorber layer is generally deposited on a Ru capping layer over a multilayer mirror, and Ru has been shown to etch spontaneously in an oxygen plasma.[21] Thus, a nonoxygen based modification approach is needed. Here, an Ni ALE process is proposed based on surface nitridation by a nitrogen plasma to form surface Ni_xN followed by FA vapor exposure to remove the Ni_xN layer.

Transition metal nitrides (TMNs) play a critical role in many applications due to properties such as their hardness and superconductivity. Joe Greene was a leading figure in the study of TMNs. He examined the synthesis by reactive magnetron sputtering of many TMNs including TiN,[22] HfN,[23] TaN,[24] and VN[25] and

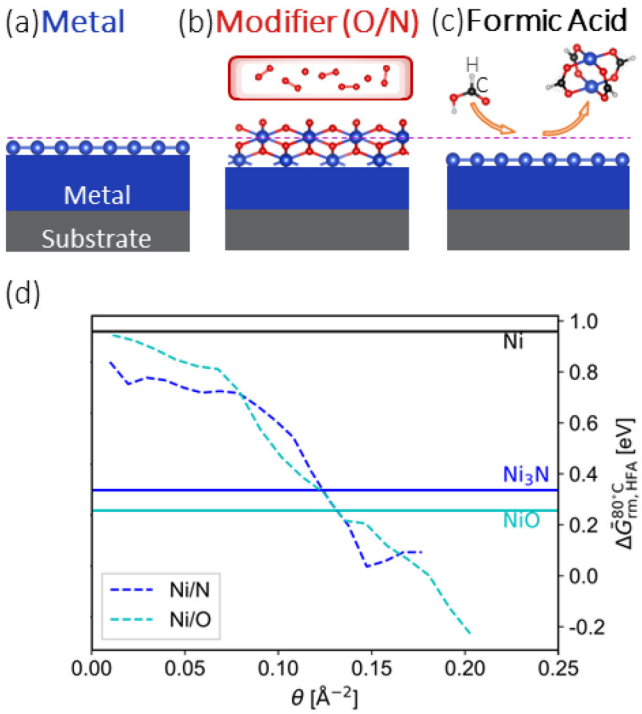

FIG. 1. (a)–(c) Schematic showing a plasma-thermal approach to ALE of metals. (a) Metal as deposited. (b) In the first half-cycle, the surface is modified by exposure to a plasma. (c) In the second half-cycle, the modified layer is removed selective to the metal by an organic vapor such as formic acid (FA). (d) Theoretical work showing that removal of Ni_3N and NiO has similar energetics. Reprinted with permission from Xia and Sautet, Chem. Mater. **33**, 6774–6786 (2021). Copyright (2021), American Chemical Society.

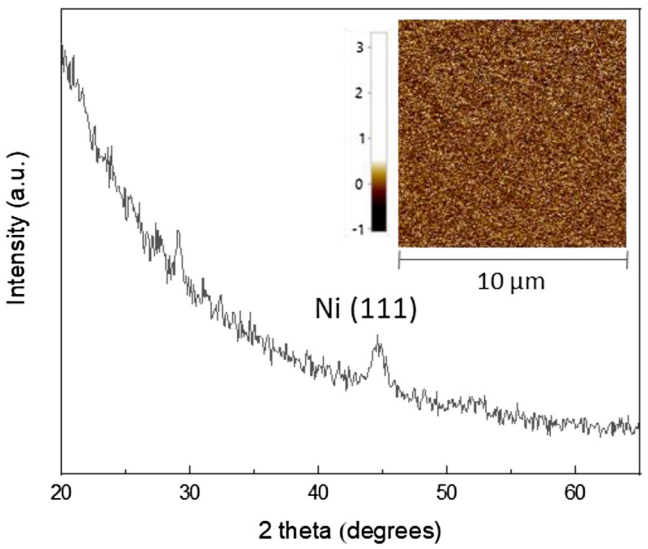

FIG. 2. XRD of the Ni thin film after deposition by PVD. The average grain size was estimated to be 5 nm based on the FWHM of the Ni (111) peak. The inset shows an AFM scan of a 10 × 10 μm^2 region, which had an RMS roughness of 0.2 nm.

studied the properties of these materials and their dependence on stoichiometry. In this work, leveraging the surface stoichiometry to create a chemical contrast between Ni_xN and Ni to enable ALE was inspired by Joe Greene's foundational work.

The feasibility of nitridation-based ALE has already been shown theoretically for Ni.[26] Figure 1(d) is a plot of the Gibbs free energy of removal by FA as a function of nitrogen/oxygen surface coverage, adapted from Ref. 26. Importantly, as nitrogen surface coverage increases, the energy of removal decreases, emphasizing that significant surface nitridation is required to achieve etching. Although the removal of the nitrided surface never quite becomes negative in this plot, the addition of subsurface nitrogen atoms, which are not included, is expected to make the removal more favorable.[27]

To experimentally realize this process, a plasma process to form the surface nickel nitride (Ni_xN) is first required. Ni_3N is a material that has been studied due to its applications as a hydrogen oxidation reaction (HOR) and hydrogen evolution reaction (HER) catalyst,[28] among other applications.[29] Deposition of Ni_3N by CVD has been shown using various nickel organometallic precursors with NH_3 and H_2 as potential coreactants.[30,31] Synthesized Ni_3N powder was characterized by neutron powder diffraction and was shown to have an ε-Fe_3N type structure based on an Ni HCP lattice with N occupying 1/3 of the octahedral interstitial sites.[32] Ni_4N,[33] Ni_2N,[34] and Ni_3N_2[35] have also been reported. In this work, the formation of Ni_xN is shown at the surface of Ni films using a remote inductively coupled plasma (ICP) reactor with a nitrogen plasma. This nitridized surface layer can be removed using FA vapor. By combining the plasma nitridation and FA vapor steps, a controllable ALE process for etching Ni is demonstrated.

II. EXPERIMENT

A. Thin film deposition

Nickel thin films were deposited in a 300 mm physical vapor deposition (PVD) system by Canon-Anelva, on bulk silicon or Ru-capped silicon wafers. The deposition process was carried out at room temperature using a 6 in. pure Ni target, using a 3000 W DC Ar plasma discharge. Crystallinity is studied with x-ray diffraction (XRD) scans in the Bragg–Brentano geometry, which is sensitive to lattice planes parallel to the film surface. An x-ray wavelength of 1.54 Å was used. The resulting XRD data are shown in Fig. 2. The most intense diffraction peak of a reference Ni film of 20 nm is located at 44° (2Θ), which is attributed to Ni (111) oriented lattice planes. The average crystal grain size can be estimated from the full width at half maximum (FWHM) of the Ni (111), using Scherrer's equation, giving a value of around 5 nm. The surface topography of the film was measured by atomic force microscopy (AFM) in the noncontact mode with an AC160 probe. The topography is shown in the inset in Fig. 2, and a smoothness of approximately 0.2 nm RMS was calculated. X-ray reflectivity, x-ray photoelectron spectroscopy (XPS), and resistivity measurements indicate that the nominal Ni film is actually composed of an interfacial layer of

NiO_x (~1.5 nm), a bulk Ni film, and then a surface layer (~1.0 nm) composed of NiO_x and $Ni(OH)_2$. XPS sputter profiling indicates a uniform metallic phase in the bulk part of the film. Due to the interfacial NiO_x, the bulk resistivity is reached for films above 15 nm thickness, reaching a value of 18 $\mu\Omega$ cm. For this work, Ni films with an initial thickness of 29 nm were used.

B. Plasma nitridation

Before nitridation, samples were sputter cleaned for 2 min using a 3 cm Kaufman ion source (Commonwealth Scientific). Ar gas was fed in at a rate of 3 SCCM such that the chamber had an operating pressure of $\sim 3 \times 10^{-5}$ Torr. An ion beam voltage of 1000 V was applied with an ion beam current of 13 mA, which led to a removal rate of about 1.5 nm/min. The ion source chamber is connected to the ICP reactor and is separated by a gate valve. Sample transfer between the chambers using a magnetically coupled transfer arm allows the sample to be loaded in the ICP chamber without breaking vacuum after sputter cleaning.

Plasma nitridation was performed in a stainless-steel ICP plasma reactor with an upper and lower chamber separated by a 0.71 in. aperture. This allows for remote processing with the sample loaded in the lower chamber and the plasma generated in the upper chamber. An inductive coil connected to a 13.5 MHz RF power source (ENI ACG-10B) is placed on top of a quartz window to supply power to the plasma. The upper chamber contains a quartz liner where the plasma is generated. The upper chamber is pumped down by a 360 l/s turbomolecular pump (Leybold Turbovac 360), while the lower chamber is connected to a 4000 l/s cryogenic pump (Cryo-Torr 8). During operation, the gate valve between the lower chamber and the cryogenic pump is closed and the chamber is pumped down only by the turbomolecular pump. Nitrogen is fed in through a mass flow controller (MKS), and the pressure is controlled by throttling the valve in between the upper chamber and the turbomolecular pump. Plasma nitridation in this reactor was carried out at 35 mTorr, 500 W power, and 0 V applied bias.

C. Vapor exposure

Vapor exposure was performed in a custom-built chamber pumped down by a mechanical roughing pump (Alcatel Adixen 2021i). FA is kept in a glass ampoule and is fed through a liquid flow controller (Horiba Stec LF-F) into a vaporizer (Horiba Stec MI-1000). Nitrogen gas is fed into the vaporizer through a mass flow controller (Horiba Stec SEC-E40). The vapor delivery lines and reaction chamber are heated by a heating tape with the temperature manually controlled through variable transformers. For the experiments in this paper, the chamber and delivery lines were heated to 80 °C and the operating pressure of the chamber was 350 Torr. The vapor chamber is not attached to the ICP system, so there was a vacuum break of at most 1 min in between each half-cycle.

D. Thin film measurements

XPS was carried out in a Kratos Axis Ultra with an Al K-α source (1486.6 eV) at an emission current of 10 mA. The take-off angle was 90°. A pass energy of 160 eV was used for the wide survey scans, and a pass energy of 40 eV was used for the detailed region scans. For nonconductive samples, the main hydrocarbon peak of the C 1s region was charge corrected to 284.8 eV, and all other peaks for that sample were corrected by the same amount. Peak fitting was carried out in CasaXPS v2.3.25 using a Shirley background, and escape depth correction was performed using the electron attenuation lengths. For XPS depth profiles, an Ar^+ ion gun was used with a source voltage of 3 kV and an extractor current of 50 μA.

Scanning electron microscopy (SEM, FEI Nova 600) was used to determine the Ni film thicknesses. These measurements were also corroborated with spectroscopic ellipsometry (SE, J. A. Woollam M-88). The ellipsometry data were fit using a harmonic oscillator model for Ni.

III. RESULTS AND DISCUSSION

The amount of surface nitridation as a function of plasma exposure time was investigated. Samples were nitridized for 1, 5, and 10 min, respectively, and the N:Ni ratio was measured by XPS using the survey spectra. As shown in Fig. 3(a), the amount of

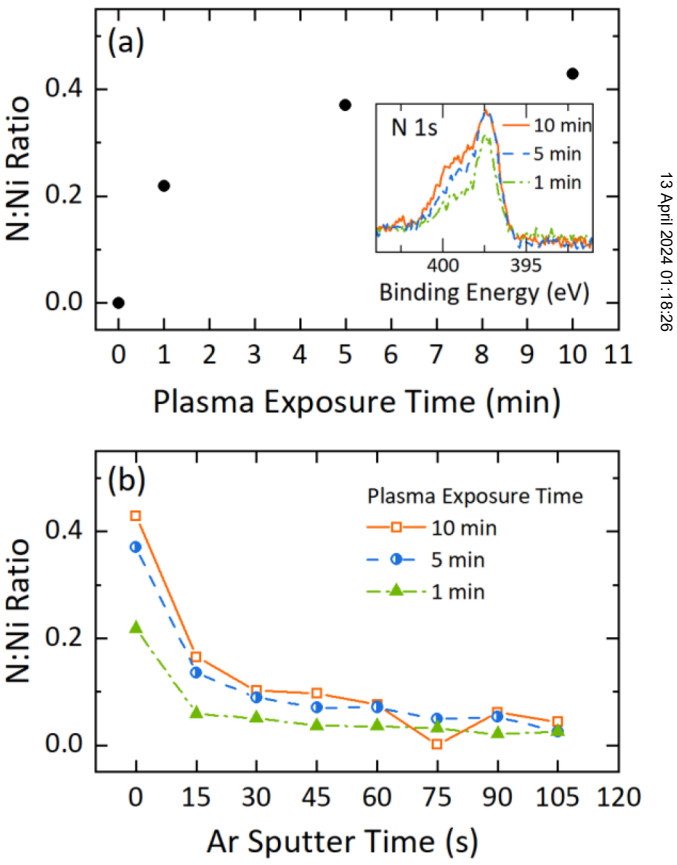

FIG. 3. (a) N:Ni ratio of Ni samples as a function of plasma exposure time, determined by XPS. The inset shows the corresponding N 1s spectra. (b) XPS depth profile of samples exposed to 1, 5, and 10 min of nitrogen plasma.

nitridation increases asymptotically with increasing exposure time. These samples were also investigated by XPS depth profiling. It should be noted that due to its lower atomic mass, N is likely preferentially sputtered over Ni, possibly distorting the compositional measurements. As seen in the depth profiles in Fig. 3(b), most of the nitrogen content of the samples is confined to the surface layer. Samples exposed to 5 and 10 min of nitrogen plasma had nitrogen penetration further into the surface than the sample exposed for only 1 min. For further experiments, a plasma nitridation time of 5 min was used. It was found that the N:Ni ratio at the surface after 5 min of plasma nitridation was 0.37, suggesting significant nitrogen incorporation at the surface, which is a prerequisite for etching.[26] Many phases of Ni_xN have been reported in the literature, with $x = 4$, 3, 2 being the most commonly observed.[34,36] These phases can be intermixed, complicating quantification. Ni_3N_2 has also been reportedly synthesized by the thermal decomposition of nickel(II) amide 2-ammoniate,[35] but it has not been observed by reactive sputtering.[34] Since an N:Ni ratio of 0.37 exceeds the ratio of Ni_3N (0.33), it is believed that the surface is composed of Ni_2N or Ni_2N intermixed with Ni_3N. This high nitrogen content Ni_2N is likely possible because the remote plasma relies on N radicals from the surface nitride while isolating the sample from energetic ions. Ni_xN is metastable and readily decomposes, so exposure to energetic ions would likely prevent the formation of Ni_2N either by sputtering or localized heating of the surface.

Figure 4 shows that, after plasma nitridation, a clear peak emerges in the XPS N 1s spectrum at a binding energy (BE) of 397.3 eV. This position is consistent with the N 1s peak of other metal nitrides, which typically have binding energies between 397 and 398 eV. This peak was fit with an asymmetric line shape due to the metallic nature of Ni_xN. In the Ni $2p_{3/2}$ region, the main asymmetric Ni peak was centered at 852.6 eV with characteristic metallic Ni satellites. It is believed that this peak is associated with Ni_2N, Ni_3N, and Ni. XPS measurements on Ni_3N by Zhang *et al.* showed the Ni_3N peak at 852.5 eV after confirming the formation of Ni_3N with XRD and Raman spectroscopy.[37] A similar spectrum was observed by Väyrynen *et al.*, and they attributed the absence of a chemical shift in the Ni $2p_{3/2}$ region to a lack of Ni-N bonds, with N only occupying interstitial sites.[38] No reference could be found for the XPS spectra of Ni_2N; however, the lack of a chemical shift in the Ni $2p_{3/2}$ region despite a prominent N 1s peak points to the Ni_2N being an interstitial compound like Ni_3N. Because of the lack of a defining Ni_xN peak in the Ni $2p_{3/2}$ region, the N 1s region was used as the primary indicator of the formation of Ni_xN. The Ni $2p_{3/2}$ and N 1s regions also show the presence of NiO, Ni_zO_yN, and $Ni(OH)_2$, likely due to exposure to ambient conditions.

Having verified successful nitridation, the removal of the nitride layer with FA was then examined. This was first tested by dipping a nitridized sample in FA solution for 1 min at 80 °C. As shown in Fig. 4, the nitride and oxynitride peaks in the N 1s region are no longer present after the FA solution dip, suggesting a complete removal of the metal nitride. Vapor phase removal was then tested. After 5 min of exposure to FA vapor, the Ni_2N and Ni_zO_yN peaks in the N 1s region are also no longer present. This indicates that the surface nitride and oxynitride were completely removed by the FA vapor, a necessary condition for the ALE process.

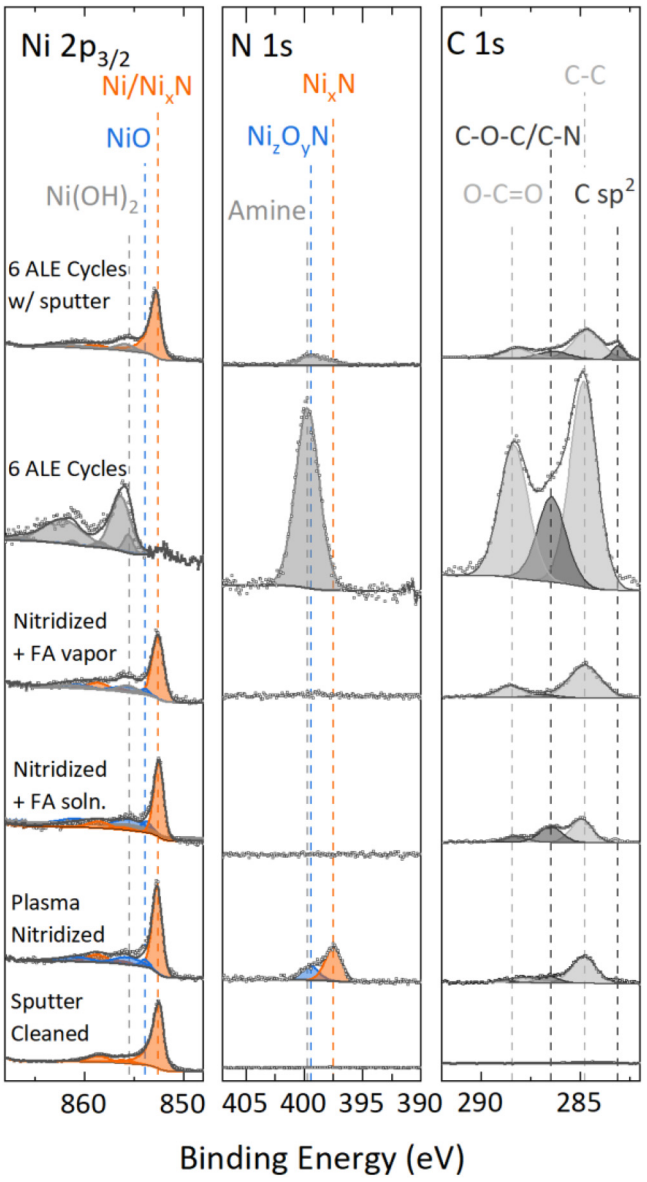

FIG. 4. XPS scans of the Ni $2p_{3/2}$, N 1s, and C 1s regions for various samples. A sputter cleaned Ni peak is shown for reference. After plasma nitridation, a Ni-N peak appears at 397.3 eV in the N 1s region. Exposure to FA in solution and vapor phase removes the nitride, as manifested by the disappearance of the Ni-N peak. A six cycle ALE process left behind residual R-N contamination on the surface. This carbonaceous buildup was prevented by incorporating a mild Ar^+ sputter step between cycles.

The presence of Ni_zO_yN did not negatively impact this removal. Indeed, since FA etches NiO, the slight oxidation of the surface was not expected to impede the process. However, to verify that the vacuum break in between the plasma process and FA vapor exposure—and the resulting surface oxidation—was not the

driving force behind the removal, the oxidation of a sputter cleaned Ni sample was examined by XPS. After sputter cleaning, the sample was left under ambient conditions for 36 h, a time much greater than the <1 min vacuum break. After ambient exposure, the Ni $2p_{3/2}$ XPS spectrum showed that the sample surface had oxidized, with a $Ni(OH)_2$ peak appearing. However, the metallic Ni $2p_{3/2}$ peak still comprised 69% of the total Ni $2p_{3/2}$ intensity, and using the Hill equation to estimate the oxidized thickness yielded an $Ni(OH)_2$ thickness of ~0.8 nm.[39] This is less than the etch rate per cycle observed from the ALE process (reported later), and, thus, the ALE process reported here is not driven by oxidation during the vacuum break. The etch observed must then be due to plasma nitridation.

An experiment was then conducted to determine the effects of FA exposure time on the removal of the nitride. Samples were sputter cleaned, nitridized for 5 min in the remote nitrogen plasma, and then exposed to FA vapor for various times. The results of this experiment are shown in Fig. 5 with the intensity of the fitted N 1s Ni_2N peak at 397.3 eV plotted as a function of FA exposure time. The N 1s spectra are included as an inset in the figure. At 5 min of FA, most of the metal nitride was removed, and by 10 min, the Ni_2N peak was barely distinguishable above the noise. For all exposure times, the Ni_zO_yN peak at a BE of 399.2 eV disappears, suggesting rapid, complete removal of oxynitride at the surface. However, a new peak at 399.8 eV emerges, which is ascribed to amines or other R-N groups, which have N 1s peaks

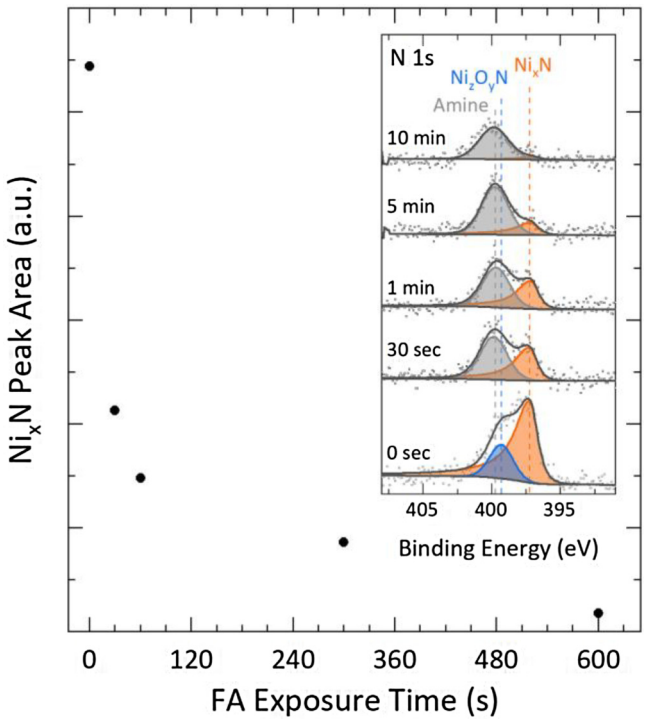

FIG. 5. Ni_2N peak area as a function of FA exposure time. The N 1s spectra are included in the inset.

with BEs ranging from about 399.5–403 eV.[40] There appear to be competing reactions between the etching of Ni_2N/Ni_zO_yN and the formation of R-N carbon species. At the same FA exposure time of 5 min, the N 1s peak at 399.8 eV in Fig. 5 was not observed in Fig. 4. This discrepancy is due to an FA refill in between the two sets of experiments, likely resulting in an unintentional higher dose of FA for the experiments in Fig. 5.

An Ni sample was then exposed to six full ALE cycles consisting of plasma nitridation and 5 min FA vapor exposure. The XPS spectra of this experiment are shown in Fig. 4. Notably, there was a significant increase in the amount of carbon on the surface accompanied by a continued strong R-N peak in the N 1s region at 399.8 eV. Work by Mameli *et al.* has shown that organic etchants in ALE can decompose on the surface, leaving behind carbon residues that can be removed in an oxygen plasma.[41] Indeed, the previously reported ALE of Ni using an oxygen plasma and FA did not observe problematic buildup, corroborating these results.[5] This is likely because oxygen plasma can react with the surface carbon to form gaseous CO or CO_2. However, the process proposed in this work avoids oxygen plasma in order to protect the Ru capping layer. The remote N_2 plasma here relies predominantly on N radicals to nitridize the surface, which apparently do not react to form volatile carbon species. Instead, the carbonaceous residue is left behind to act as an etch stop that reduces etching.

To prevent the buildup of the carbon on the surface, a light 2 min Ar^+ sputter step using the Kaufman ion source was added in between the FA vapor exposure and the subsequent plasma nitridation. This was performed at a much lower ion beam voltage (200 V) than the sputter clean carried out at the beginning of each experiment (1000 V), and SEM showed the negligible etching of Ni at this lower voltage. This three step ALE process was then tested. The XPS spectra of this sample are also shown in Fig. 4. The peak attributed to C sp^2 in the C 1s region is likely a result of the ion beam optics, which are made of graphite, slightly sputtering onto the surface. However, overall, the inclusion of the sputtering step shows a substantial decrease in the amount of residual carbon. In addition to preventing the carbon buildup, the directional Ar^+ ion beam could also impart anisotropy to the process. The N radicals of the remote plasma will modify Ni isotropically. However, the carbon buildup on the surface could prevent this. If the Ar^+ ion beam is used to anistropically remove the residual carbon on the horizontal surfaces but leaves behind residual C on the sidewalls, this could effectively induce anisotropy.

Ni film thickness as a function of number of cycles is shown in Fig. 6 for the ALE process both with and without sputtering in between cycles. The data point at 0 cycles is the thickness of the Ni film after receiving the initial 2 min Ar^+ ion beam clean at 1000 V. For the ALE with intercycle sputtering, an etch rate of 1.3 ± 0.17 nm/cycle was calculated. The surface roughness was also measured. As reported in the Sec. II, the RMS roughness of the Ni films postdeposition was 0.2 nm. The initial sputter clean at 1000 V increased the surface roughness to 1.0 nm. After six cycles of the three step ALE process, the RMS roughness decreased slightly to 0.9 nm. Surface smoothing is a common phenomenon in thermal ALE processes, and the slight smoothing observed in this work is likely due to the thermal FA vapor half-cycle, which etches isotropically.

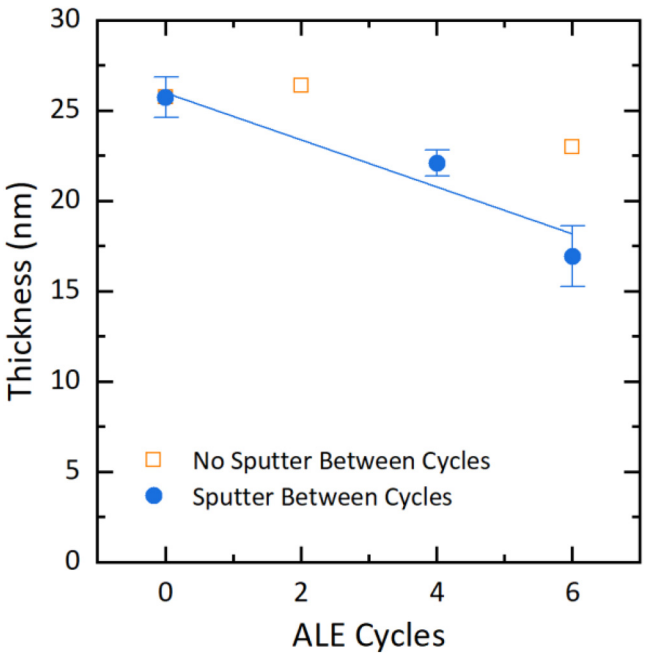

FIG. 6. Thickness change in Ni samples as a function of ALE cycles both with and without a sputter step in between cycles. Error bars represent the standard deviation of four replicates for the data point at 0 and three replicates for the other data points.

IV. SUMMARY AND CONCLUSIONS

Plasma nitridation of Ni surfaces using a remote ICP plasma was successfully demonstrated. It was shown that FA in both the solution phase and vapor phase can remove the surface nitride layer. Combining plasma nitridation and FA vapor created an ALE process that built up significant surface contamination over time, necessitating a mild Ar^+ ion beam sputtering step in between cycles to remove the buildup. The three step ALE process—plasma nitridation, FA vapor, and ion beam sputtering—yielded an etch rate of 1.3 ± 0.17 nm/cycle. Further work is underway to evaluate the selectivity of Ru and effects on surface roughness. This new nitridation-based approach to plasma-thermal ALE also opens the way for future investigation into etching Ni_xAl_y alloys by a similar mechanism for EUV and interconnect applications.

ACKNOWLEDGMENTS

The authors acknowledge funding from the National Science Foundation Award Nos. 1805112 and 2212981. J.P.C. acknowledges the mentorship and support by Joe Greene within AVS. The authors acknowledge the use of instruments at the UCLA Nanolab, IMEC's 300 mm Pilot line for performing part of the operations needed for substrate preparation, as well as Xiaoyu Piao for optimizing the Ni deposition process.

AUTHOR DECLARATIONS

Conflict of Interest

The authors have no conflicts to disclose.

Author Contributions

Taylor G. Smith: Conceptualization (equal); Data curation (equal); Formal analysis (equal); Investigation (equal); Writing – original draft (equal); Writing – review & editing (equal). **Ali M. Ali:** Data curation (supporting); Formal analysis (supporting); Investigation (supporting). **Jean-François de Marneffe:** Project administration (equal); Resources (supporting); Supervision (equal); Writing – review & editing (supporting). **Jane P. Chang:** Conceptualization (equal); Funding acquisition (lead); Investigation (equal); Project administration (lead); Supervision (lead); Writing – review & editing (equal).

DATA AVAILABILITY

The data that support the findings of this study are available from the corresponding author upon reasonable request.

REFERENCES

[1]V. Philipsen *et al.*, Proc. SPIE **10143**, 1014310 (2017).
[2]F. Scholze, C. Laubis, K. V. Luong, and V. Philipsen, Proc. SPIE **10466**, 1044609 (2017)
[3]L. Chen, D. Ando, Y. Sutou, D. Gall, and J. Koike, Appl. Phys. Lett. **113**, 183503 (2018).
[4]J. P. Soulié, Z. Tőkei, J. Swerts, and C. Adelmann, *2020 IEEE International Interconnect Technology Conference (IITC)*, San Jose, CA, 5–8 October 2020 (IEEE, New York, 2020), pp. 151–153.
[5]X. Sang, E. Chen, and J. P. Chang, J. Vac. Sci. Technol. A **38**, 042603 (2020).
[6]J. A. Murdzek, A. Lii-Rosales, and S. M. George, Chem. Mater. **33**, 9174 (2021).
[7]M. Konh, C. He, X. Lin, X. Guo, V. Pallem, R. L. Opila, A. V. Teplyakov, Z. Wang, and B. Yuan, J. Vac. Sci. Technol. A **37**, 021004 (2019).
[8]N. K.-C. Chen, N. D. Altieri, T. Kim, E. Chen, T. Lill, M. Shen, and J. P. Chang, J. Vac. Sci. Technol. A **35**, 05C305 (2017).
[9]J. K.-C. Chen, N. D. Altieri, T. Kim, T. Lill, M. Shen, and J. P. Chang, J. Vac. Sci. Technol. A **35**, 05C304 (2017).
[10]E. Mohimi, X. I. Chu, B. B. Trinh, S. Babar, G. S. Girolami, and J. R. Abelson, ECS J. Solid State Sci. Technol. **7**, P491 (2018).
[11]A. I. Abdulagatov, J. L. Partridge, V. Sharma, C. L. Dezelah, and S. M. George, AVS 67, Virtual Symposium, Virtual Symposium (2021).
[12]R. Sheil, J. M. P. Martirez, X. Sang, E. A. Carter, and J. P. Chang, J. Phys. Chem. C **125**, 1819 (2021).
[13]X. Lin, M. Chen, A. Janotti, and R. Opila, J. Vac. Sci. Technol. A **36**, 051401 (2018).
[14]M. Konh, A. Janotti, and A. Teplyakov, J. Phys. Chem. C **125**, 7142 (2021).
[15]B. M. Coffey, H. C. Nallan, J. R. Engstrom, and J. G. Ekerdt, ACS Appl. Mater. Interfaces **12**, 50985 (2020).
[16]B. M. Coffey, H. C. Nallan, J. R. Engstrom, C. H. Lam, and J. G. Ekerdt, Chem. Mater. **32**, 6035 (2020).
[17]B. M. Coffey, H. C. Nallan, and J. G. Ekerdt, J. Vac. Sci. Technol. A **39**, 012601 (2021).
[18]K. J. Kanarik, S. Tan, and R. A. Gottscho, J. Phys. Chem. Lett. **9**, 4814 (2018).
[19]A. Lii-Rosales, A. S. Cavanagh, A. Fischer, T. Lill, and S. M. George, Chem. Mater. **33**, 7719 (2021).
[20]X. Sang and J. P. Chang, J. Vac. Sci. Technol. A **38**, 042604 (2020).
[21]C. C. Hsu, J. W. Coburn, and D. B. Graves, J. Vac. Sci. Technol. A **24**, 1 (2005).
[22]J. E. Sundgren, B. O. Johansson, A. Rockett, S. A. Barnett, and J. E. Greene, AIP Conf. Proc. **149**, 95 (1986).

[23]H.-S. Seo, T.-Y. Lee, I. Petrov, J. E. Greene, and D. Gall, J. Appl. Phys. **97**, 083521 (2005).
[24]C.-S. Shin, D. Gall, Y.-W. Kim, P. Desjardins, I. Petrov, J. E. Greene, M. Odén, and L. Hultman, J. Appl. Phys. **90**, 2879 (2001).
[25]A. B. Mei, R. B. Wilson, D. Li, D. G. Cahill, A. Rockett, J. Birch, L. Hultman, J. E. Greene, and I. Petrov, J. Appl. Phys. **115**, 214908 (2014).
[26]Y. Xia and P. Sautet, Chem. Mater. **33**, 6774 (2021).
[27]X. Sang, Y. Xia, P. Sautet, and J. P. Chang, J. Vac. Sci. Technol. A **38**, 043005 (2020).
[28]W. Ni, A. Krammer, C.-S. Hsu, H. M. Chen, A. Schüler, and X. Hu, Angew. Chem., Int. Ed. **58**, 7445 (2019).
[29]S. H. Gage, B. G. Trewyn, C. V. Ciobanu, S. Pylypenko, and R. M. Richards, Catal. Sci. Technol. **6**, 4059 (2016).
[30]Z. Li, R. G. Gordon, V. Pallem, H. Li, and D. V. Shenai, Chem. Mater. **22**, 3060 (2010).
[31]E. Lindahl, M. Ottosson, and J.-O. Carlsson, ECS Trans. **25**, 365 (2009).
[32]A. Leineweber, H. Jacobs, and S. Hull, Inorg. Chem. **40**, 5818 (2001).
[33]I. M. Neklyudov and A. N. Morozov, Phys. B **350**, 325 (2004).
[34]G. J. W. R. Dorman and M. Sikkens, Thin Solid Films **105**, 251 (1983).
[35]G. W. Watt and D. D. Davies, J. Am. Chem. Soc. **70**, 3753 (1948).
[36]H. A. Wriedt, Bull. Alloy Phase Diagrams **6**, 558 (1985).
[37]N. Zhang *et al.*, Angew. Chem., Int. Ed. **58**, 15895 (2019).
[38]K. Väyrynen *et al.*, Phys. Status Solidi A **216**, 1900058 (2019).
[39]J. M. Hill, D. G. Royce, C. S. Fadley, L. F. Wagner, and F. J. Grunthaner, Chem. Phys. Lett. **44**, 225 (1976).
[40]A. V. Naumkin, A. Kraut-Vass, S. W. Gaarenstroom, and C. J. Powell, NIST Standard Reference Database Number 20. National Institute of Standards and Technology (2000).
[41]A. Mameli, M. A. Verheijen, A. J. M. Mackus, W. M. M. Kessels, and F. Roozeboom, ACS Appl. Mater. Interfaces **10**, 38588 (2018).